Article

Unconventional magnons in collinear magnets dictated by spin space groups

https://doi.org/10.1038/s41586-025-08715-7

Received: 23 July 2023

Accepted: 29 January 2025

Published online: 12 March 2025

Open access

Check for updates

Xiaobing Chen[1,2], Yuntian Liu[1], Pengfei Liu[1], Yutong Yu[1], Jun Ren[1], Jiayu Li[1], Ao Zhang[1] & Qihang Liu[1,2,3]✉

Magnonic systems provide a fertile playground for bosonic topology[1], for example, Dirac[2–6] and Weyl[7,8] magnons, leading to a variety of exotic phenomena such as charge-free topologically protected boundary modes[6,7], the magnon thermal Hall effect[9] and the magnon spin Nernst effect[10]. However, their understanding has been hindered by the absence of fundamental symmetry descriptions of magnetic geometries and spin Hamiltonians primarily governed by isotropic Heisenberg interactions. The ensuing magnon dispersions enable gapless magnon band nodes that go beyond the scenario of representation theory of the magnetic space groups[11,12], thus referred to as unconventional magnons. Here we developed spin space group[13–17] theory to elucidate collinear magnetic configurations, classifying the 1,421 collinear spin space groups into 4 types, constructing their band representations and providing a comprehensive tabulation of unconventional magnons, such as duodecuple points, octuple nodal lines and charge-4 octuple points. On the basis of the MAGNDATA database[18], we identified 498 collinear magnets with unconventional magnons, among which more than 200 magnon band structures were obtained by using first-principles calculations and linear spin wave theory. In addition, we evaluated the influence of the spin–orbit-coupling-induced exchange interaction in these magnets and found that more than 80 per cent are predominantly governed by the Heisenberg interactions, indicating that the spin space group serves as an ideal framework for describing magnon band nodes in most 3*d*, 4*d* and half-filled 4*f* collinear magnets.

Finding unconventional magnets that contain topological magnons is an area of high interest and demand, with potential applications in next-generation ultrafast spintronic devices and quantum computing. However, extending the success of topological band theory and material diagnosis from electrons to magnons faces a significant challenge in the fundamental symmetry description of magnetic materials. The conventional framework for describing the symmetry of magnetic materials and designing magnon band nodes is based on magnetic space groups (MSGs)[11,12]. These groups completely lock the rotational operations in spin space and real space. Nevertheless, the magnon dispersions, especially in collinear magnets with small spin–orbit coupling (SOC) effects (for example, the Dzyaloshinskii–Moriya interaction[19,20]), predominantly depend on the isotropic Heisenberg exchange interaction. As a result, even though the material candidates for experimental measurements are rare, the existing experimentally observed magnon spectra still cannot be entirely explained by MSGs. Examples include the observed Dirac and sextuple points in collinear antiferromagnet (AFM) Cu_3TeO_6 (refs. 3,4) and the two-fold nodal plane in collinear ferromagnet (FM) gadolinium[21].

Spin space groups (SSGs), which were first proposed in the 1960s (yet overlooked until the recent development of AFM spintronics[22–38]), provide a framework that allows for decoupling of spatial and spin operations, and an examination of the symmetries associated with magnon dispersions[39,40]. In this work, we develop the SSG theory describing collinear magnetic configurations, which are typically dictated by the Heisenberg exchange interaction, and apply it to a comprehensive search of unconventional magnons in real materials. We categorize the 1,421 collinear SSGs into four types, corresponding to all the type I, III and IV MSGs but with more spatial-free spin symmetries and thus different band representations. By employing the representation theory, we not only capture the band degeneracies to reconcile the results of previous experiments but also tabulate all possible unconventional magnons, such as duodecuple (12-fold) nodal point, charge-4 octuple (8-fold) point, octuple nodal line, quadruple nodal plane and altermagnetic-splitting chiral magnons. We further conduct high-throughput ab initio calculations on the magnon band dispersions and representations for 348 computable collinear magnets within the MAGNDATA database, which adopts experimentally confirmed magnetic structures. On the basis of an efficient and systematic diagnosis, we identify more than 200 unconventional magnonic materials by the calculated bilinear magnetic exchange coefficients and magnon dispersions. By comparing the results with and without SOC, we evaluate the magnitude of anisotropic interactions and thus the validity of unconventional magnons within the SSG scenario. Finally, we

[1]Department of Physics and Guangdong Basic Research Center of Excellence for Quantum Science, Southern University of Science and Technology, Shenzhen, China. [2]Quantum Science Center of Guangdong–Hong Kong–Macao Greater Bay Area (Guangdong), Shenzhen, China. [3]Guangdong Provincial Key Laboratory of Computational Science and Material Design, Southern University of Science and Technology, Shenzhen, China. ✉e-mail: liuqh@sustech.edu.cn

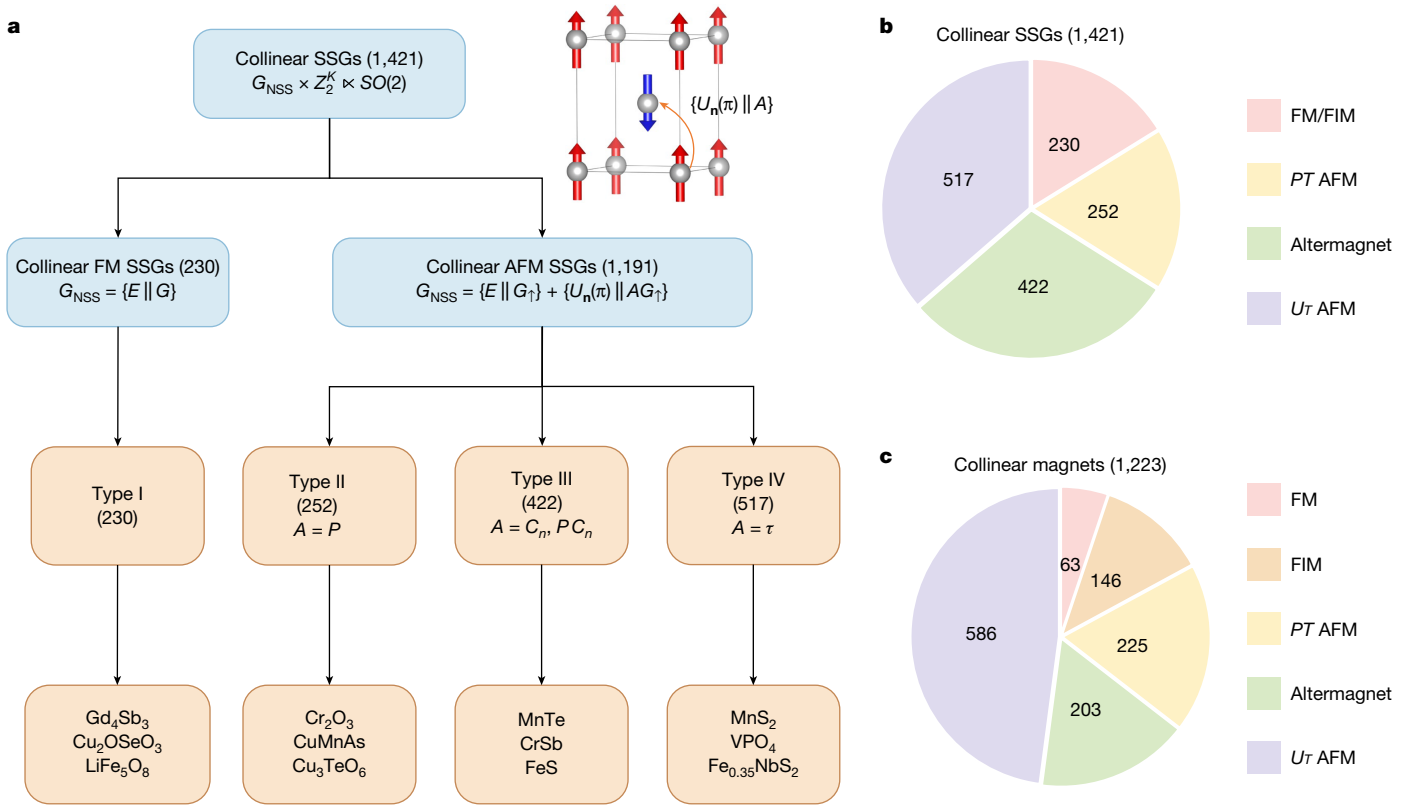

Fig. 1 | Classification of 1,421 SSGs for collinear magnets. a, For a collinear FM, the SSG $G_{NSS} = \{E\|\|G\}$ can be constructed from the space group G. For a collinear AFM, the sublattice space group $G_\uparrow$, the space group G of the magnetic cell and the space operation A (see inset of magnetic structure) that connects different magnetic sublattices are necessary for constructing $G_{NSS} = \{E\|\|G_\uparrow\} + \{U_n(\pi)\|\|AG_\uparrow\}$. Collinear AFM SSGs can be further classified into three categories based on the space operation A. The number in the parentheses represents the number of the corresponding SSGs. The last row lists the material candidates for each category. τ, fractional lattice translation; P, spatial inversion; C_n, spatial rotations. **b**, Statistics of the collinear SSGs characterizing four types of collinear magnet. **c**, Statistics of the five types of collinear magnet in the MAGNDATA database.

provide the full array of data of collinear SSG theory, including general positions, spin Wyckoff positions, spin Brillouin zones, little co-groups of wavevectors, band representations and the magnon dispersions of calculated magnets in our homemade online program and database FINDSPINGROUP (https://findspingroup.com/).

Collinear SSGs

Beginning with 90 spin point groups describing collinear magnetic orders[14], 1,421 SSGs for collinear magnets can be constructed by group extension[15]. A typical SSG operation is written as $\{O_s\|\|O_r\}$, where O_s and O_r denote the operation in spin space and real space, respectively. In general, SSGs can be expressed as $G_S = G_{NSS} \times G_{SO}$, where G_{SO} stands for the spin-only group that contains only spin operations $\{O_s\|\|E\}$ (E is the identity operation), and G_{NSS} stands for the non-trivial SSG that contains no pure spin operations[41]. For collinear magnetic structures, $G_{SO} = Z_2^K \ltimes SO(2)$, where $SO(2) = \{U_z(\phi),\ \phi \in [0, 2\pi)\}$ contains full spin rotations U with the rotation angle ϕ along the spin axis z, and $Z_2^K = \{E, TU_n(\pi) = K\}$ contains the product of the time reversal T and a two-fold spin rotation about any axis $\mathbf{n}$ perpendicular to the z axis[14].

For collinear FM materials with only one type of magnetic sublattice, the non-trivial SSG is given by $G_{NSS} = \{E\|\|G\}$, where G is the space group (230 in total). These SSGs are also sufficient to describe the symmetry of a collinear ferrimagnet (FIM) that contains multiple spin sublattices but without any symmetry connecting them. On the other hand, the definition of AFM used here, followed by Louis Néel, refers to a magnetic-ordered state with zero net magnetic moment where the magnetic sublattices with opposite spins are crystallographic equivalent[42]. For a collinear AFM with two sublattices carrying opposite spins, G_{NSS} is obtained by group extension $\{E\|\|G_\uparrow\} + \{U_n(\pi)\|\|AG_\uparrow\}$, where the sublattice space group $G_\uparrow$ contains all spatial symmetries that do not exchange atoms from different sublattices; $\{U_n(\pi)\|\|A\}$ is the symmetry operation that combines the exchange of the two sublattices (A) and spin reversal ($U_n(\pi)$).

In analogy with the construction of type I, III and IV MSGs, 1,421 collinear SSGs are constructed, including 230 type I SSGs describing collinear FMs and FIMs, and 1,191 SSGs describing collinear AFMs. Compared with 674 type III MSGs, we further categorize collinear SSGs using $\{U_n(\pi)\|\|A\}$, including 252 type II SSGs with $A = P$ (P represents the space inversion), and 422 type III SSGs with $A = C_n, PC_n$ ($n = 2, 4$) (C_n, PC_n stand for n-fold symmorphic or non-symmorphic space rotations and rotoinversions, respectively). Such classification naturally leads to the separation of conventional PT-symmetric AFMs with two-fold spin-degenerate bands (type II SSGs) and the recently emerged altermagnets[27] with AFM-induced spin splitting[23,24] (type III SSGs). Besides, there are 517 type IV SSGs describing AFMs with $A = \tau$ (τ represents the fractional lattice translation). All collinear SSGs are tabulated in Supplementary Information section 2 and are summarized in Fig. 1a. Although the 1,421 collinear SSGs show one-to-one correspondence with the 1,421 MSGs, they manifest more spin symmetries, including spin $SO(2)$, $TU_n(\pi)$ and $\{U_n(\pi)\|\|A\}$, which are crucial for more band degeneracies beyond the regime of MSGs (see a detailed comparison in Supplementary Information section 1). We list the SSGs of all collinear magnets in MAGNDATA in our online database FINDSPINGROUP.

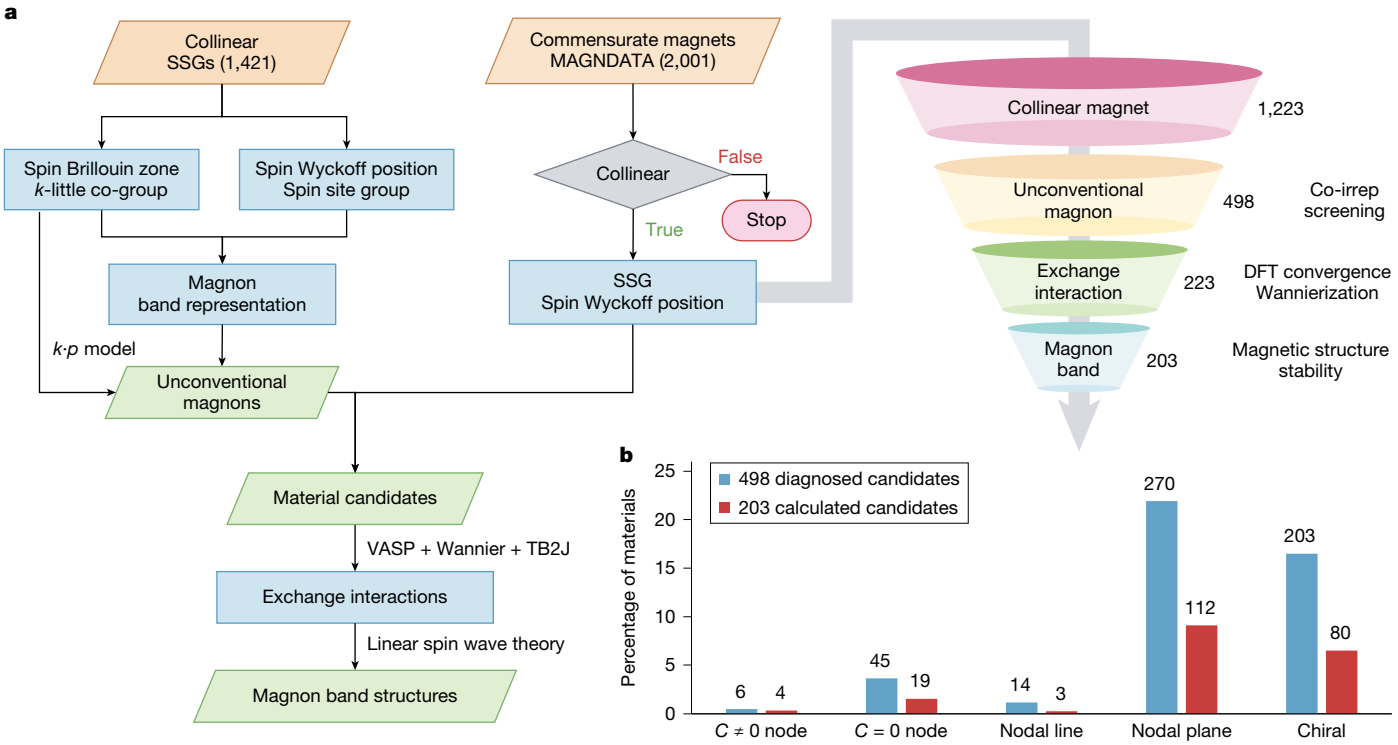

Fig. 2 | Workflow for the construction of the unconventional magnon database. a, First, 1,223 collinear magnets were identified from the MAGNDATA database. Second, after the identification of the SSG, co-irrep screenings were performed to obtain the material candidates hosting unconventional magnons. Third, high-throughput calculations were performed to obtain all bilinear exchange interactions. Finally, an unconventional-magnon database with 203 magnon band structures and identified band representations was constructed. **b**, Statistics of five types of unconventional magnon in the collinear magnets from the MAGNDATA database, including: (1) chiral quasiparticles ($C \neq 0$), including C-4 octuple, C-4 sextuple, C-8 Dirac and C-2 triple magnons; (2) topological charge-neutral ($C = 0$) quasiparticles, including duodecuple, octuple, sextuple and triple magnons; (3) octuple nodal line magnons; (4) quadruple nodal plane magnons; and (5) altermagnetic-splitting chiral magnons.

Workflow

We briefly discuss the procedure to obtain all types of unconventional magnon and their realization in collinear magnets documented in MAGNDATA (Fig. 2a). For 1,421 collinear SSGs, we establish the database for general positions, spin Wyckoff positions, spin site groups, spin Brillouin zones, little co-groups of wavevectors k and magnon band representations (Methods). For material realization, we adopt the MAGNDATA database, which contains more than 2,000 commensurate magnetic structures determined by neutron scattering measurements. By spin group symmetry identification, we filter out 1,223 collinear magnets (Fig. 1b) with their SSGs and spin Wyckoff positions of magnetic ions. According to the corresponding band representations, we identify 498 materials hosting unconventional magnons, including 5 FMs, 17 FIMs and 476 AFMs, which can be further classified into 56 PT AFMs, 203 altermagnets and 217 $U\tau$ AFMs.

After excluding magnetic structures with fractional occupancy or more than 80 atoms in the spin primitive cell, we perform density functional theory and Wannier projection calculations on 348 materials. After filtering out the cases that fail to converge and Wannierize, we obtain the bilinear magnetic exchange coefficients of 223 collinear magnets by using the TB2J code. The magnon band structures of the Heisenberg spin Hamiltonians are calculated by the linear spin wave theory. Specifically, Holstein–Primakoff transformation $S^+ \approx \sqrt{2S}a$, $S^- \approx \sqrt{2S}a^\dagger$, $S^z = S - a^\dagger a$ connects the magnon creation $a^\dagger$ (annihilation a) operator with the electron annihilation S^- (creation S^+) operator[43]. Finally, we obtain the unconventional magnons and corresponding irreducible co-representations (co-irreps) in 203 collinear magnets, whereas the magnon Hamiltonians of the other 20 systems are negative-definite, leading to the magnetic instability. More computational details can be found in Methods.

Catalogue of unconventional magnons

For collinear magnets, the spin-only group $Z_2^K \ltimes SO(2)$ leads to three main types of symmetry resulting in extra degeneracies of magnon bands. (1) Unitary spin space symmetry (USS): the combination of $SO(2)$ with unitary $\{U_n(\pi)||A\}$ symmetry pairs two conjugated one-dimensional irreducible representations (irreps) for $S^\pm$ into a two-dimensional irrep in spin space. (2) Antiunitary spin space symmetry (ASS): combination of $SO(2)$ with antiunitary $\{T||A\}$ pairs two conjugated one-dimensional irreps for $S^\pm$ into a two-dimensional co-irrep in spin space. (3) Antiunitary real-space symmetry (ARS): antiunitary $\{TU_n(\pi)||E\}$ symmetry pairs two conjugated irreps of real-space operations (Methods).

We next note several features of the magnon band degeneracies based on the co-irreps of collinear SSG. (1) Despite the absence of T, type I SSGs have the same band degeneracy and topology as the corresponding space group G combining T owing to $\{TU_n(\pi)||E\}$ symmetry. This is also applicable in searching electron orbital multiplets of a collinear FM[44]. (2) For collinear SSGs describing an AFM, magnon band structures are doubly degenerate throughout the Brillouin zone for all type II and type IV SSGs, because of ASS $\{T||P\}$ and USS $\{U_n(\pi)||\tau\}$ at an arbitrary k point, respectively. (3) The topological charges at nodal points formed by two opposite-spin branches are opposite for type II SSGs, but identical for type IV SSGs. (4) Magnon band structures with type III SSGs show AFM-induced chirality splitting, the magnonic analogue of spin splitting in altermagnets[38]. Therefore, the unconventional magnons can be classified into five categories (Fig. 2b). The correspondence between co-irreps and unconventional magnons in all collinear SSGs is provided in Supplementary Information section 3.

Figure 2b summarizes the statistics of material candidates hosting the five categories of unconventional magnons. Notably, about 40% of the collinear magnets have at least one type of unconventional magnon.

Table 1 | Summary of unconventional magnons identified in prototypical candidate materials

SSG	*k* point	Band representation at *k*	Type	Material
220.220.1.1 ($I^1\bar{4}^1 3^1 d^{\infty m}1$)	H (1, 1, 1)	$H_4^S H_5^S(6)$	SP	Gd_4Sb_3 (FM)
	Γ (0, 0, 0)	$\Gamma_4^S(3), \Gamma_5^S(3)$	TP	
227.227.1.1 ($F^1 d^1 \bar{3}^1 m^{\infty m}1$)	Γ (0, 0, 0)	$\Gamma_5^{S,+}(3)$	TP	$Lu_2V_2O_7$[a] (FM)
212.212.1.1 ($P^1 4_3^1 3^1 2^{\infty m}1$)	Γ (0, 0, 0)	$\Gamma_4^S(3), \Gamma_5^S(3)$	*C*-2 TP	$LiFe_5O_8$ (FIM)
218.222.1.1 ($P^{\bar{1}} n^{\bar{1}} \bar{3}^1 n^{\infty m}1$)	R (1/2, 1/2, 1/2)	$R_4^S R_5^S(12)$	DCP	$Pr_5Mo_3O_{16}$[b] (*PT* AFM)
199.206.1.1 ($I^{\bar{1}} a^{\bar{1}} \bar{3}^{\infty m}1$)	Γ (0, 0, 0)	$\Gamma_4^S(6)$	C_2-2 SP	Cu_3TeO_6[a] (*PT* AFM)
	H (1, 1, 1)	$H_4^S(6)$		
159.190.1.1 ($P^{\bar{1}} \bar{6}^1 2^1 c^{\infty m}1$)	A (0, 0, 1/2)	$A_3^S A_3^S(8)$	OP	FeS (altermagnet)
62.63.2.1 ($P_B^1 n^1 m^1 a^{\infty m}1$)	Q (1/2, 1/2, *w*)	$Q_1^S Q_1^S(8)$	ONL	Mn_5Si_3 (*Uτ* AFM)
	W (*u*, *v*, 1/2)	$W_1^S W_2^S(4)$	QNPL	
19.18.2.1 ($P_c^1 2_1^1 2_1^1 2_1^{\infty m}1$)	R (1/2, 1/2, 1/2)	$R_1^S R_1^S(8)$	*C*-4 OP	$Fe_{0.35}NbS_2$ (*Uτ* AFM)
	L (1/2, *v*, *w*)	$L_1^S L_1^S(4)$	QNPL net	
	N (*u*, 1/2, *w*)	$N_1^S N_1^S(4)$		
	W (*u*, *v*, 1/2)	$W_1^S W_1^S(4)$		
195.197.2.1 ($P_I^1 2^1 3^{\infty m}1$)	Γ (0,0,0)	$\Gamma_2^S \Gamma_3^S(4)$	*C*-8 DP	$LaMn_3Cr_4O_{12}$ (*Uτ* AFM)
	Γ (0,0,0)	$\Gamma_4^S(6)$	*C*-4 SP	
	R (1/2,1/2,1/2)	$R_4^S(6)$	*C*-4 SP	

[a]The nodal feature has been experimentally observed. [b]The material is synthesized in experiment, but the magnetic structure is artificially imposed. *C*-*n* means that the topological charge *C* is $|C| = n$. C_2-*m* means that the monopole charge $C_2 = (C_\uparrow - C_\downarrow)/2$ is $|C_2| = m$. The letters *u*, *v*, *w* in the second column stand for the coordinates in momentum space. DCP, duodecuple point; ONL, octuple nodal line; OP, octuple point; SP, sextuple point; QNPL, quadruple nodal plane; DP, Dirac point; TP, triple point.

The two major types are quadruple nodal plane magnon (22.08%) and altermagnetic chiral magnon (16.60%). This is consistent with that the proportion of altermagnets and *Uτ* AFMs is relatively large in collinear magnets with unconventional magnons in Fig. 1c. In Table 1, we list some representative materials with their SSGs, co-irreps and magnon node topology, and the diagnosis results of all 498 materials with unconventional magnon are provided in Supplementary Information section 4.

Representative materials

We present calculated materials manifesting various unconventional magnons in each type of SSG, including their degeneracy and node topology. The calculated magnon band structures of all the 203 candidates are provided in Supplementary Information section 5. We begin with sextuple and triple points in type I collinear SSG $I^1\bar{4}^1 3^1 d^{\infty m}1$ in FM Gd_4Sb_3 (Fig. 3a–c). Since collinear magnets cannot have cubic MSGs, any triple or sextuple magnons are thus absent within the regime of MSG. However, we find triple magnons at the Γ point, indicating that the SSG maintains the cubic nature of the lattice. In addition, owing to the ARS $\{TU_{\mathbf{n}}(\pi)||C_{2z}|\tau_{y/2}\}$, two triple magnons stick together forming a sextuple magnon at the boundary of the Brillouin zone (H point). This is a typical case where the decoupled spin and space rotations in type I SSGs provide a more fertile platform for quasiparticles than MSGs. We note that similar ARS was found to protect the two-fold nodal plane in collinear FM gadolinium[21].

Compared with the collinear FM, spin space can lead to additional degeneracy by USS and/or ASS in a collinear AFM. The presented example is *PT* AFM Cu_3TeO_6 (Fig. 3d–f), whose magnon dispersion were measured by inelastic neutron scattering experiments[3,4]. Specifically, the magnon bands are doubly degenerate throughout the whole Brillouin zone, with several sextuple and Dirac magnons identified at the Γ, P and H points. These features are all beyond the regime of MSG, where the corresponding MSG $R\bar{3}'$ predicts a non-degenerate band at an arbitrary *k* point and at most two-fold band crossings at any high-symmetry points (Supplementary Information section 7.3.2). In sharp contrast, these band degeneracies are perfectly described using co-irreps of the type II cubic SSG $I^{\bar{1}} a^{\bar{1}} \bar{3}^{\infty m}1$. In particular, the little group $^{\bar{1}}m^{\bar{1}}\bar{3}^{\infty m}1$ allows sextuple magnons at the Γ and H points with a C_2-2 monopole charge (Methods) and thus the hidden magnon thermal Hall effect (Table 1). We further note that the highest dimension of the symmetry-protected magnon bands in type II SSGs is 12. A representative example is the R point in experimentally synthesized $Pr_5Mo_3O_{16}$, where a collinear AFM order is implemented (Supplementary Information section 7.3.5).

Another interesting case is the octuple magnon, which is found at the A point in type III SSG $P^{\bar{1}}\bar{6}^{\bar{1}}2^1 c^{\infty m}1$ in FeS (Fig. 3g–i). Such an octuple magnon is also the synergistic effect of the ASS $(\{U_{\mathbf{n}}(\pi)||m_z|\tau_{z/2}\})$ and ARS $(\{T||C_{2x}|0\})$. Moreover, the bands off the high-symmetry point are non-degenerate, leading to AFM-induced magnon chirality splitting along, for example, the Γ–A and A–K directions. We expect that magnon chirality splitting in collinear AFM can lead to the appearance of non-zero Berry curvature, magnon orbital angular momentum and the magnon nonlinear thermal Hall effect in the absence of SOC, which will further expand the scope of the relevant field of spintronics[45–47]. We list all the 203 diagnosed altermagnets and the momentum position of magnon chirality splitting (also electronic spin splitting) from MAGNDATA in Supplementary Information section 4.6 and our online database FINDSPINGROUP.

The magnon quasiparticles carry various topological charges, some of which are absent in all encyclopaedias of MSGs[48–50] but protected by SSG symmetries. One striking case is the charge-4 (*C*-4) octuple magnons (Fig. 3j–l) in collinear $Fe_{0.35}NbS_2$ with a type IV SSG $P_a^1 2_1^1 2_1^1 2_1^{\infty m}1$. Owing to the $\{U_{\mathbf{n}}(\pi)||E|\tau\}$ and ARS $\{T||C_{2z}|\tau_{x/2}\}$ of the little group of $k_z = \pi$ plane, the magnon bands form quadruple Z–U–R–T nodal plane and octuple quasiparticle at the R point. Different from type II SSGs, the sign of Berry curvature from the two pairs of four-fold degenerate bands connected by $\{U_{\mathbf{n}}(\pi)||E|\tau\}$ are identical for type IV SSGs, resulting in *C*-4 octuple magnons as the superposition of two *C*-2 Dirac points at R. Furthermore, three perpendicular *k* planes (k_x, k_y, $k_z = \pi$) intersecting at the R point form a quadruple nodal plane network (Supplementary Information section 7.3.4). We predict cases of magnon band topology such as *C*-4 sextuple and *C*-8 Dirac magnons as summarized in Supplementary Information section 4.

SOC effects

To evaluate the applicability of collinear SSGs in diagnosing unconventional magnons, we fully consider SOC effects by calculating the bilinear magnetic exchange interactions, including antisymmetric Dzyaloshinskii–Moriya interaction (*D*), exchange anisotropy (J^{ani}) and off-diagonal symmetric anisotropy (*Γ*), and compare them with the isotropic Heisenberg exchange interaction (*J*) in 223 candidate materials. Notably, single-ion anisotropy is excluded in our analysis because in collinear magnets it does not affect the symmetry of the magnon Hamiltonian, the band representations or the nodal topology (Supplementary Information section 7).

Table 2 shows that in 82% of the calculated collinear magnets, the Dzyaloshinskii–Moriya interaction, exchange anisotropy (for example, Kitaev interaction) and off-diagonal symmetric anisotropy are at least an order of magnitude smaller than the Heisenberg interaction, indicating the validity of SSG for these systems. Specifically, 87% of the 3*d* and 4*d* magnets are dominated by Heisenberg interactions, whereas the

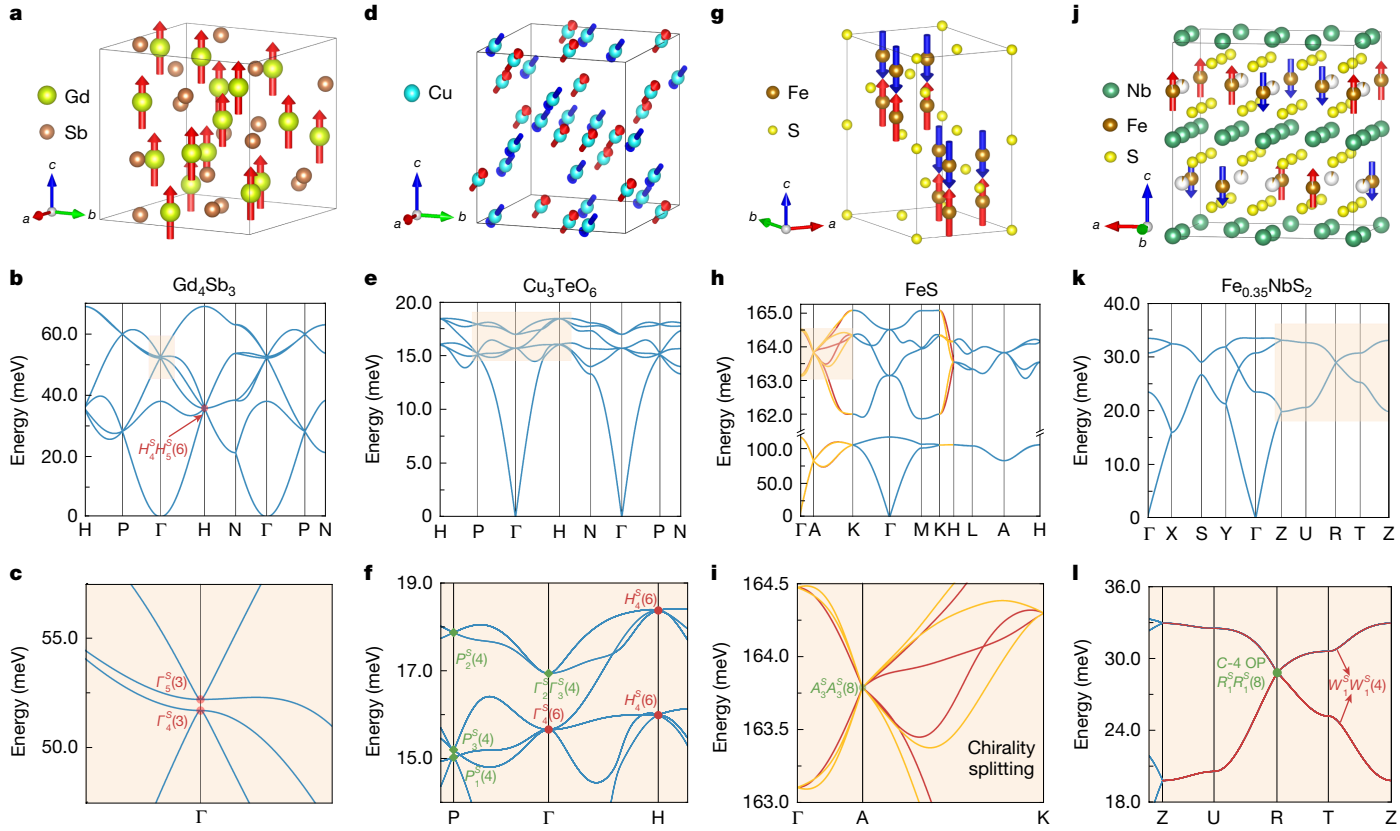

Fig. 3 | Material candidates hosting unconventional magnons. a–**c**, The magnetic structure (**a**), magnon band structure (**b**) with a zoomed-in view (**c**) of collinear FM Gd_4Sb_3, which has six-, four- and three-fold band crossings. **d**–**f**, The same as **a**–**c**, but for collinear AFM Cu_3TeO_6 with 6-fold band crossing at the Γ and H points. **g**–**i**, The same as **a**–**c**, but for altermagnet FeS, which has octuple degeneracy at the A point and magnon chirality splitting along the A–K line. The red and yellow lines represent the magnon chirality splitting bands with magnon spin $S = 1$ and $S = -1$, respectively, and the blue lines represent spin-degenerate bands. **j**–**l**, The same as **a**–**c**, but for collinear AFM $Fe_{0.35}NbS_2$ with *C*-4 octuple magnons at the R point. The red lines indicate the quadruple Z–U–R–T nodal plane. A schematic of the Brillouin zone for each candidate can be found in Supplementary Information section 7.

remaining ones have strong Dzyaloshinskii–Moriya interactions, such as the reported altermagnet $Fe_2Mo_3O_8$ with a Dzyaloshinskii–Moriya-interaction-induced magnon polaron[51]. In addition, the half-filled 4*f* magnets are also largely compatible with the framework of SSGs, such as Gd^{3+} in $GdAlO_3$ and GdAgSn. However, the MSG framework could be more applicable for the 5*d* and 5*f* magnets owing to their strong Dzyaloshinskii–Moriya interaction or exchange anisotropy. These results indicate that SSG serves as an ideal framework for describing magnon band nodes in most 3*d*, 4*d* and 4*f* collinear magnets. Detailed information regarding the calculated exchange interactions for 223 candidates is available in Supplementary Information section 6. More discussions on band topology, nonlinear magnons and their SOC effects can be found in Methods.

Table 2 | Statistics of bilinear exchange interactions with SOC

Magnetic ions	Materials	<10% $\|J\|$			*J* dominated
		$\|D\|$	$\|J^{ani}\|$	$\|\Gamma\|$	
3*d*	194	175	182	189	169
4*d*	7	5	5	6	5
4*f*	12	11	10	11	9
5*d*	6	1	0	3	0
5*f*	4	1	0	3	0
Total	223	193	197	212	183

The second column presents the number of collinear magnets classified by the outermost shell of magnetic ions in the first column. The third to fifth columns evaluate the number of materials in which the magnitude of the Dzyaloshinskii–Moriya interaction (D), exchange anisotropy (J^{ani}) and anisotropic symmetric (Γ) terms does not exceed 10% of that of the Heisenberg term (J), respectively. The last column gives the number of J-dominated magnets, in which none of $|D|$, $|J^{ani}|$ and $|\Gamma|$ exceeds 10% $|J|$. Detailed statistical methods and exchange parameters can be found in Supplementary Information section 6.

The main outcome of this work is twofold. First, we present a comprehensive representation theory of 1,421 collinear SSGs, which includes the spin Wyckoff positions, spin Brillouin zones and band representations associated with each wavevector. Such a framework allows for the full tabulation of unconventional quasiparticles beyond the MSGs. Second, we provide a dictionary of more than 200 candidate materials that host unconventional magnons, identified through high-throughput calculations. The integration of SSGs and the collinear magnets listed in the MAGNDATA database facilitates efficient and systematic characterization of magnons showing non-trivial nodal topology. By virtue of this, the unconventional magnons have the potential to host topologically protected, uncharged surface states, leaving fruitful transport and neutron scattering signatures for experiments.

Online content

Any methods, additional references, Nature Portfolio reporting summaries, source data, extended data, supplementary information, acknowledgements, peer review information; details of author contributions and competing interests; and statements of data and code availability are available at https://doi.org/10.1038/s41586-025-08715-7.

1. McClarty, P. A. Topological magnons: a review. *Annu. Rev. Condens. Matter Phys.* **13**, 171–190 (2022).
2. Li, K. et al. Dirac and nodal line magnons in three-dimensional antiferromagnets. *Phys. Rev. Lett.* **119**, 247202 (2017).
3. Yao, W. et al. Topological spin excitations in a three-dimensional antiferromagnet. *Nat. Phys.* **14**, 1011–1015 (2018).
4. Bao, S. et al. Discovery of coexisting Dirac and triply degenerate magnons in a three-dimensional antiferromagnet. *Nat. Commun.* **9**, 2591 (2018).
5. Chen, L. et al. Topological spin excitations in honeycomb ferromagnet CrI_3. *Phys. Rev. X* **8**, 041028 (2018).
6. Yuan, B. et al. Dirac magnons in a honeycomb lattice quantum *XY* magnet $CoTiO_3$. *Phys. Rev. X* **10**, 011062 (2020).
7. Li, F.-Y. et al. Weyl magnons in breathing pyrochlore antiferromagnets. *Nat. Commun.* **7**, 12691 (2016).
8. Mook, A., Henk, J. & Mertig, I. Tunable magnon Weyl points in ferromagnetic pyrochlores. *Phys. Rev. Lett.* **117**, 157204 (2016).
9. Hwang, K., Trivedi, N. & Randeria, M. Topological magnons with nodal-line and triple-point degeneracies: implications for thermal Hall effect in pyrochlore iridates. *Phys. Rev. Lett.* **125**, 047203 (2020).
10. Cheng, R., Okamoto, S. & Xiao, D. Spin Nernst effect of magnons in collinear antiferromagnets. *Phys. Rev. Lett.* **117**, 217202 (2016).
11. Karaki, M. J. et al. An efficient material search for room-temperature topological magnons. *Sci. Adv.* **9**, eade7731 (2023).
12. Corticelli, A., Moessner, R. & McClarty, P. A. Identifying and constructing complex magnon band topology. *Phys. Rev. Lett.* **130**, 206702 (2023).
13. Brinkman, W. F. & Elliott, R. J. Theory of spin-space groups. *Proc. R. Soc. A* **294**, 343–358 (1966).
14. Liu, P. et al. Spin-group symmetry in magnetic materials with negligible spin–orbit coupling. *Phys. Rev. X* **12**, 021016 (2022).
15. Chen, X. et al. Enumeration and representation theory of spin space groups. *Phys. Rev. X* **14**, 031038 (2024).
16. Xiao, Z. et al. Spin space groups: full classification and applications. *Phys. Rev. X* **14**, 031037 (2024).
17. Jiang, Y. et al. Enumeration of spin-space groups: toward a complete description of symmetries of magnetic orders. *Phys. Rev. X* **14**, 031039 (2024).
18. Gallego, S. V. et al. MAGNDATA: towards a database of magnetic structures. I. The commensurate case. *J. Appl. Crystallogr.* **49**, 1750–1776 (2016).
19. Dzyaloshinsky, I. A thermodynamic theory of "weak" ferromagnetism of antiferromagnetics. *J. Phys. Chem. Solids* **4**, 241–255 (1958).
20. Moriya, T. Anisotropic superexchange interaction and weak ferromagnetism. *Phys. Rev.* **120**, 91–98 (1960).
21. Scheie, A. et al. Dirac magnons, nodal lines, and nodal plane in elemental gadolinium. *Phys. Rev. Lett.* **128**, 097201 (2022).
22. Zelezny, J., Zhang, Y., Felser, C. & Yan, B. Spin-polarized current in noncollinear antiferromagnets. *Phys. Rev. Lett.* **119**, 187204 (2017).
23. Hayami, S., Yanagi, Y. & Kusunose, H. Momentum-dependent spin splitting by collinear antiferromagnetic ordering. *J. Phys. Soc. Jpn* **88**, 123702 (2019).
24. Yuan, L.-D. et al. Giant momentum-dependent spin splitting in centrosymmetric low-*Z* antiferromagnets. *Phys. Rev. B* **102**, 014422 (2020).
25. Ma, H.-Y. et al. Multifunctional antiferromagnetic materials with giant piezomagnetism and noncollinear spin current. *Nat. Commun.* **12**, 2846 (2021).
26. Liu, P., Zhang, A., Han, J. & Liu, Q. Chiral Dirac-like fermion in spin–orbit-free antiferromagnetic semimetals. *The Innovation* **3**, 100343 (2022).
27. Šmejkal, L., Sinova, J. & Jungwirth, T. Beyond conventional ferromagnetism and antiferromagnetism: a phase with nonrelativistic spin and crystal rotation symmetry. *Phys. Rev. X* **12**, 031042 (2022).
28. Guo, P. J. et al. Eightfold degenerate fermions in two dimensions. *Phys. Rev. Lett.* **127**, 176401 (2021).
29. Shao, D. F. et al. Spin-neutral currents for spintronics. *Nat. Commun.* **12**, 7061 (2021).
30. Bai, H. et al. Observation of spin splitting torque in a collinear antiferromagnet RuO_2. *Phys. Rev. Lett.* **128**, 197202 (2022).
31. Bose, A. et al. Tilted spin current generated by the collinear antiferromagnet ruthenium dioxide. *Nat. Electron.* **5**, 267–274 (2022).
32. Feng, Z. et al. An anomalous Hall effect in altermagnetic ruthenium dioxide. *Nat. Electron.* **5**, 735–743 (2022).
33. Shao, D. F. et al. Neel spin currents in antiferromagnets. *Phys. Rev. Lett.* **130**, 216702 (2023).
34. Zhu, Y.-P. et al. Observation of plaid-like spin splitting in a noncoplanar antiferromagnet. *Nature* **626**, 523–528 (2024).
35. Krempaský, J. et al. Altermagnetic lifting of Kramers spin degeneracy. *Nature* **626**, 517–522 (2024).
36. Ghorashi, S. A. A., Hughes, T. L. & Cano, J. Altermagnetic routes to Majorana modes in zero net magnetization. *Phys. Rev. Lett.* **133**, 106601 (2024).
37. Yang, J., Liu, Z.-X. & Fang, C. Symmetry invariants and classes of quasiparticles in magnetically ordered systems having weak spin–orbit coupling. *Nat. Commun.* **15**, 10203 (2024).
38. Šmejkal, L. et al. Chiral magnons in altermagnetic RuO_2. *Phys. Rev. Lett.* **131**, 256703 (2023).
39. Brinkman, W. Magnetic symmetry and spin waves. *J. Appl. Phys.* **38**, 939–943 (1967).
40. Corticelli, A., Moessner, R. & McClarty, P. A. Spin-space groups and magnon band topology. *Phys. Rev. B* **105**, 064430 (2022).
41. Litvin, D. B. Spin point groups. *Acta Crystallogr. A* **33**, 279–287 (1977).
42. Néel, L. *Propriétés magnétiques des ferrites; ferrimagnétisme et antiferromagnétisme*. *Ann. Phys.* **12**, 137–198 (1948).
43. Holstein, T. & Primakoff, H. Field dependence of the intrinsic domain magnetization of a ferromagnet. *Phys. Rev.* **58**, 1098–1113 (1940).
44. Li, J. et al. Designing light-element materials with large effective spin–orbit coupling. *Nat. Commun.* **13**, 919 (2022).
45. Neumann, R. R., Mook, A., Henk, J. & Mertig, I. Orbital magnetic moment of magnons. *Phys. Rev. Lett.* **125**, 117209 (2020).
46. Liu, Y. et al. Switching magnon chirality in artificial ferrimagnet. *Nat. Commun.* **13**, 1264 (2022).
47. Fishman, R. S., Gardner, J. S. & Okamoto, S. Orbital angular momentum of magnons in collinear magnets. *Phys. Rev. Lett.* **129**, 167202 (2022).
48. Yu, Z. M. et al. Encyclopedia of emergent particles in three-dimensional crystals. *Sci. Bull.* **67**, 375–380 (2022).
49. Liu, G.-B. et al. Systematic investigation of emergent particles in type-III magnetic space groups. *Phys. Rev. B* **105**, 085117 (2022).
50. Zhang, Z. et al. Encyclopedia of emergent particles in type-IV magnetic space groups. *Phys. Rev. B* **105**, 104426 (2022).
51. Bao, S. et al. Direct observation of topological magnon polarons in a multiferroic material. *Nat. Commun.* **14**, 6093 (2023).

Methods

Band representation theory for SSGs

Band representations are constructed from the atomic limit as introduced by Zak[52]. Building on Zak's theory, the theory of topological quantum chemistry and symmetry indicators were used in electronic topological diagnosis, where thousands of materials with topological electronic bands have been successfully identified[53–59]. Here we extend it to the SSG. First, we construct the spin site group $G_S^{\mathbf{q}}$ of the SSG G_S, the corresponding character table and the irreps of orbit basis $\rho_{S^\pm}^{\mathbf{q}}$, where $\mathbf{q}$ is any point in the unit cell of magnetic lattice. Among these spin site groups, only 32 FM spin point groups can support non-zero magnetic moments and carry magnon. Second, to induce full band representations $\rho_{S^\pm}=\rho_{S^\pm}^{\mathbf{q}}\uparrow G_S$, we seek a coset decomposition of $G_S^{\mathbf{q}}$. All orbits of the Wyckoff position $\{\mathbf{q}_\alpha=g_\alpha\mathbf{q}_1|g_\alpha\in G_S\}$, $\alpha=1, 2, \ldots, n$ with multiplicity n of the Wyckoff position are derived. The SSG element g_α, combined with the translation $\mathbb{T}$, generate the decomposition of G_S with respect to the $G_S^{\mathbf{q}}$:

$$G_S=\bigcup_\alpha g_\alpha(G_S^{\mathbf{q}}\ltimes\mathbb{T}) \tag{1}$$

The full band representation $\rho_{S^\pm}=(\rho_{S^\pm}^{\mathbf{q}}\uparrow G_S)$ is induced from orbital representation $\rho_{S^\pm}^{\mathbf{q}}$, then we restrict it to band representations of k-little groups $\rho_{S^\pm}^{\mathbf{k}}=\rho_{S^\pm}\downarrow G_S^{\mathbf{k}}$ with ingredients:

$$\chi_{\rho_{S^\pm}^{\mathbf{k}}}(g)=\begin{cases}\sum_\alpha \mathrm{e}^{-\mathrm{i}[R(g)k\cdot t_{\alpha\alpha}]}\chi_{\rho_{S_\alpha^\pm}^{\mathbf{q}}}(g_\alpha^{-1}\{E||E|-t_{\alpha\alpha}\}gg_\alpha) & g\in G_S^{\mathbf{q}}\\ 0 & g\notin G_S^{\mathbf{q}}\end{cases} \tag{2}$$

where $t_{\alpha\alpha}=g\mathbf{q}_\alpha-\mathbf{q}_\alpha$. In this step, the character table of the unitary part of $G_S^{\mathbf{k}}$ is also constructed. At last, we perform sum rules[60] to account for the introduction of antiunitary operations and the band representation $\rho_{S^\pm}^{\mathbf{k}}$ in spin Brillouin zone is determined. The bases of magnon bands $S^\pm$ transform as the irreps of the spin site groups of the magnetic ions. For collinear magnets, the spin site group always has $SO(2)$ spin rotation symmetry, $S^\pm$ thus transform as $m_s=\pm1$ irreps of $SO(2)$ in spin space (m_s represents the spin angular momentum), whereas the real-space part only provides the identity irrep for $S^\pm$.

Two mechanisms of extra two-fold degeneracy provided by spin space

For a collinear AFM, G_S has the form of $(\{E||G_\uparrow\}+\{U_{\mathbf{n}}(\pi)||AG_\uparrow\})\times Z_2^K\ltimes SO(2)$. Here we briefly show how the combination of $SO(2)$ spin symmetry with $\{U_{\mathbf{n}}(\pi)||A\}$ or $\{T||A\}$ will pair two one-dimensional irreps into a two-dimensional irrep for $S^\pm$ in spin space.

Despite the pure space rotations ($G_\uparrow^k$) and pure spin rotations from $SO(2)$ symmetry in the little group G_S^k, three symmetry operations account for the two-fold degeneracy in spin space, including $\{U_{\mathbf{n}}(\pi)||A\}$, $\{T||A\}$ and $\{TU_{\mathbf{n}}(\pi)||E\}$. Here we show how these operations act with the $U_{\mathbf{z}}(\phi)$ in the $\{S^+, S^-\}$ basis.

The matrix representations of spin rotations and the time reversal are written as:

$$D(U_z(\phi))=\begin{pmatrix}\mathrm{e}^{-\mathrm{i}\phi}&0\\0&\mathrm{e}^{\mathrm{i}\phi}\end{pmatrix},\ D(U_x(\pi))=\begin{pmatrix}0&1\\1&0\end{pmatrix},\ D(T)=\begin{pmatrix}0&-1\\-1&0\end{pmatrix}K,$$

where K is the complex conjugation operator, and we use $\mathbf{n}=x$.

For $\{U_x(\pi)||A\}$:

$$\begin{aligned}&\{U_{\mathbf{x}}(\pi)||A\}\{U_{\mathbf{z}}(\phi)||E\}(\{U_{\mathbf{x}}(\pi)||A\})^{-1}=\{U_{\mathbf{z}}(-\phi)||E\}\\&\Rightarrow(\{E||G_\uparrow^k\}+\{U_{\mathbf{n}}(\pi)||AG_\uparrow^k\})\ltimes SO(2)\cong\{E||G_\uparrow^k\}\times D_\infty\end{aligned} \tag{3}$$

where D_∞ provides two-dimensional irreps for $S^\pm$.

For $\{T||A\}$:

$$(\{T||A\}\{U_{\mathbf{z}}(\phi)||E\})^2\begin{pmatrix}\psi_{i,S^+}(k)\\\psi_{i,S^-}(k)\end{pmatrix}=\begin{pmatrix}e^{2i\phi}\psi_{i,S^+}(k)\\e^{-2i\phi}\psi_{i,S^-}(k)\end{pmatrix} \tag{4}$$

where the time reversal binds two conjugated one-dimensional irreps in spin space into a two-dimensional co-irrep.

For $\{TU_{\mathbf{x}}(\pi)||E\}$:

$$(\{TU_{\mathbf{x}}(\pi)||E\}\{U_{\mathbf{z}}(\phi)||E\})^2\begin{pmatrix}\psi_{i,S^+}(k)\\\psi_{i,S^-}(k)\end{pmatrix}=\begin{pmatrix}\psi_{i,S^+}(k)\\\psi_{i,S^-}(k)\end{pmatrix} \tag{5}$$

$\{TU_{\mathbf{x}}(\pi)||E\}$ cannot contribute to the new degeneracy.

Therefore, we can conclude that both $\{U_{\mathbf{n}}(\pi)||A\}$ and $\{T||A\}$ can lead to the emergence of two-dimensional irreps in spin space. More details on band representations of collinear SSGs and the construction of magnonic band representation for SSG $I^{\bar{1}}a^{\bar{1}}\bar{3}^{\infty m}1$ (Cu_3TeO_6 case) can be found in Supplementary Information section 1.6.

Database for collinear SSG symmetry

Starting from 1,421 collinear SSGs, we establish the position-space description of collinear SSGs, where the spin site groups for all spin Wyckoff positions can be defined and characterized by 90 collinear spin point groups. Among these groups, only 32 FM spin point groups support non-zero magnetic moments, resulting in a reduction of the total number of spin Wyckoff positions from 12,481 to 6,368. Meanwhile, we introduce a momentum-space description for collinear SSGs, exhausting the spin Brillouin zones and high-symmetry k points using 24 mapped centrosymmetric symmorphic space groups. Subsequently, by employing band representation theory for SSGs as stated earlier, we derive the irreducible little co-representations of magnons in collinear SSGs and enumerate all band representations hosting unconventional magnons. Finally, we construct $k\cdot p$ effective models around the degenerate points and evaluate the node topology characterized by chiral charge or monopole charge, identifying all unconventional magnons beyond the scope of MSGs. The general positions, spin Wyckoff positions, spin site groups, spin Brillouin zones, k-little co-groups and magnon band representations for all collinear SSGs are available in our online database FINDSPINGROUP.

Density functional theory calculations

All density functional theory (DFT) calculations herein were performed using the projector augmented wave method, implemented in the Vienna Ab initio Simulation Package (VASP)[61,62]. The generalized gradient approximation of the Perdew–Burke–Ernzerhof-type exchange-correlation potential[63] was adopted. For all candidate materials, we used a cut-off energy of 500 eV, which typically leads to numerical convergence. We used Γ-centred Monkhorst–Pack meshes[64], with the standard for each direction being the product of the number of k points and a lattice length greater than 45 Å. For the d- and f-electron magnetic atoms, the initial magnetic moments were set to 5 μ_B and 7 μ_B, respectively. To include the effect of electron correlation, the DFT + U approach within the rotationally invariant formalism[65] was performed with the U_{eff} values based on the reported value from literature, which are provided in Supplementary Information section 5 for each material. To get an accurate determination of the exchange interactions, a self-consistency convergence within 10^{-7} eV was achieved in our calculations. Tight-binding models were constructed from DFT bands using the WANNIER90 package[66,67], and then the TB2J code[68] was used to extract the magnetic exchange parameters. The spin-exchange cut-off distance was set to truncate when the absolute value of the remaining Heisenberg exchange coefficients J is one-thousandth of the largest J value or numerically less than 0.001 meV. Detailed parameters of

Heisenberg exchange interactions for calculating the magnon band structure can be found in Supplementary Information section 6.

Magnon band structure calculations

The magnon band structures were all calculated using the linear spin wave theory and the Heisenberg spin Hamiltonian. The ground-state spin Hamiltonian can be changed into quadratic Hamiltonian by performing the Holstein–Primakoff transformation and Fourier transformation:

$$H = \sum_k \psi^\dagger(k) H(k) \psi(k) \tag{6}$$

where $\psi^\dagger(k) = (a_{k1}^\dagger \ldots a_{km}^\dagger a_{-k1} \ldots a_{-km})^T$, $H(k) = \begin{pmatrix} h(k) & g(k) \\ g(k)^\dagger & h(-k)^T \end{pmatrix}$

$$h(k)_{ab} = S\left[\sum_{R_{ij}} (\alpha_{ab} J_{\tau_a, \tau_b + R_{ij}}) \cdot \mathrm{e}^{\mathrm{i}kR_{ij}} - \delta_{ab} \sum_{R_{ij}, c} (\gamma_{ac} J_{\tau_a, \tau_c + R_{ij}})\right] \tag{7}$$

$$g(k)_{ab} = S \sum_{R_{ij}} (\lambda_{ab} J_{\tau_a, \tau_b + R_{ij}}) \cdot \mathrm{e}^{\mathrm{i}kR_{ij}} \tag{8}$$

where δ_{ab} is the Kronecker delta, and R and τ represent the lattice translation vector and the position of magnetic ions in the lattice basis, respectively. When $\mathbf{S}_a$ is parallel to $\mathbf{S}_b$, $\alpha_{ab} = 1$, $\gamma_{ab} = 1$ and $\lambda_{ab} = 0$; when $\mathbf{S}_a$ is antiparallel to $\mathbf{S}_b$, $\alpha_{ab} = 0$, $\gamma_{ab} = -1$ and $\lambda_{ab} = -1$.

On the basis of the above, the eigenvalues and eigenvectors of magnon Hamiltonian can be calculated by diagonalizing $H(k) \cdot I_-$, where $I_- = \begin{pmatrix} I_m & 0 \\ 0 & -I_m \end{pmatrix}$, and I_m is the m-directional identity matrix, where m represents the number of magnetic ions in a primitive cell under SSG.

Topological charges $H(k)$

We characterize the topology of the degenerate point by calculating the topological charge. For the nodal point, we calculate the Wilson loops on a sphere enclosing the nodal point[69,70]:

$$W(\theta) = \oint A(k) \mathrm{d}k \tag{9}$$

where θ is the polar angle of the sphere, and $A(k) = \mathrm{i}\langle\psi(k)|\nabla|\psi(k)\rangle$ is the Berry connection.

Now we show the different symmetry operations on $A(k)$:

$$PA(k) = -A(-k),\ TA(k) = A(-k),\ UA(k) = A(k) \tag{10}$$

As a result, the topological charge is zero at P-symmetric k points as $PW(\theta) = W(\pi - \theta)$, where Wilson loop is symmetric about the $\theta = \pi/2$ plane. This conclusion can be generalized to PC_n-invariant k point, where C_n is any proper space rotation. However, the time reversal T and spin rotation U does not give any constrains on the topological charge.

For collinear FMs, when the k-little group is chiral, it can host a non-zero topological charge. For collinear AFMs, the magnon Hamiltonian can be separated into two spin channels with spin angular momentum $S = \pm 1$, the two degenerate spin channels should be connected by TA or UA. If the k-little sublattice group $G_\uparrow^k$ is chiral, it can host a non-zero topological charge $C_\uparrow$ in the spin-up channel. The two spin channels can have identical or opposite topological charges when the two sublattices are connected by proper or improper A. In the former, the topological charge will be doubled as $C = 2C_\uparrow$, whereas $C = 0$ in the latter. For the compensated charge with improper A, we can define a monopole charge $C_2 = (C_\uparrow - C_\downarrow)/2$.

Therefore, the nodal points of two degenerate branches have opposite (identical) topological charges for type II (IV) SSGs owing to the PT ($U\tau$) symmetry in the whole-spin Brillouin zone. For type III SSGs, if $G_\uparrow^k$ is chiral and the k-little group G^k contain TA and UA operation, the two magnon branches will degenerate with doubled or compensated topological charge when A is proper or improper. However, when the k-little group does not contain TA and UA operations, the two magnon branches will split and the sign of topological charge in two channels is irrelevant.

Detailed information about the non-zero topological charges of magnonic irreps in collinear SSGs at symmetry-protected degeneracies is provided on our online program FINDSPINGROUP.

Band topology and nonlinear magnons

For collinear magnets, there exists an effective time-reversal symmetry $TU_n(\pi)$ that squares to one. Consequently, magnons in collinear magnets fall into the symmetry class AI of the Altland–Zirnbauer tenfold classification for topological insulators and superconductors, which does not support strong topological insulating phase in three dimensions[71,72]. Recent studies have shown that SOC-free weak topological insulators could exist in altermagnets[73]. In contrast, under nonlinear spin wave theory, the introduction of magnon–magnon interaction does not break the $SO(2)$ symmetry in collinear magnets. Thus, it does not change the band degeneracy, although it may cause band renormalization[74]. However, adding a SOC term to the collinear spin Hamiltonian typically opens a small gap, sometimes rendering the emergence of symmetry class AII and $\mathbb{Z}_2$ gapped topological phase. For example, the introduction of a Dzyaloshinskii–Moriya interaction in pyrochlore, honeycomb and kagome FMs can transform Dirac magnons into topological magnon bands[75–77]. In this case, the description of SSGs is still useful in that it can be used to search the SOC-induced small gap, which is often the perquisite of magnon topological materials, such as Chern insulators and axion insulators. Furthermore, the incorporation of the Dzyaloshinskii–Moriya interaction and magnon–magnon interactions can cause multiple topological phase transitions[78,79]. Overall, understanding the evolution from node topology to band topology with the introduction of the SOC effect and its impact on magnon transport will be valuable for the development of magnon-based spintronic devices, and is left for future studies.

Comparison between electrons and magnons in collinear SSGs

Importantly, we emphasize that although our focus is on magnon systems, the main results of unconventional quasiparticles originating from band degeneracies can be straightforwardly applied to electronic systems. In the framework of the (magnetic) space group, the double-valued representation of spin-1/2 fermions requires the so-called double group to describe an additional −1 phase of 2π rotation. In sharp contrast, the particularity of collinear SSGs renders that the dimension of the band representations for both fermions and bosons remains invariant within 4π rotation. This is because the infinite spin-only group $SO(2)$ has the double-covering group of itself, and can thus be regarded as either a single group or a double group. Therefore, $SO(2)$ always provides one-dimensional irreps labelled by spin angular momentum $m_s = \pm 1/2$ for electrons and $m_s = \pm 1$ for magnons. The only difference between fermions and bosons in collinear SSGs occurs solely within the phase in irrep matrices. Detailed information on the comparison between band representations for electrons and magnons in collinear SSGs is provided in Supplementary Information section 1.6.4.

Data availability

All data are available in the Supplementary Information and through our public website, the online program for identifying SSG symmetry and the collinear SSG-symmetry database (https://findspingroup.com/).

Code availability

All codes are available through our public website, the online program for identifying SSG symmetry and the collinear SSG-symmetry database (https://findspingroup.com/).

52. Zak, J. Band representations of space groups. *Phys. Rev. B* **26**, 3010–3023 (1982).
53. Bradlyn, B. et al. Topological quantum chemistry. *Nature* **547**, 298–305 (2017).
54. Kruthoff, J. et al. Topological classification of crystalline insulators through band structure combinatorics. *Phys. Rev. X* **7**, 041069 (2017).
55. Tang, F., Po, H. C., Vishwanath, A. & Wan, X. Comprehensive search for topological materials using symmetry indicators. *Nature* **566**, 486–489 (2019).
56. Zhang, T. et al. Catalogue of topological electronic materials. *Nature* **566**, 475–479 (2019).
57. Vergniory, M. G. et al. A complete catalogue of high-quality topological materials. *Nature* **566**, 480–485 (2019).
58. Xu, Y. et al. High-throughput calculations of magnetic topological materials. *Nature* **586**, 702–707 (2020).
59. Elcoro, L. et al. Magnetic topological quantum chemistry. *Nat. Commun.* **12**, 5965 (2021).
60. Dimmock, J. O. & Wheeler, R. G. Symmetry properties of wave functions in magnetic crystals. *Phys. Rev.* **127**, 391–404 (1962).
61. Kresse, G. & Furthmüller, J. Efficient iterative schemes for ab initio total-energy calculations using a plane-wave basis set. *Phys. Rev. B* **54**, 11169–11186 (1996).
62. Kresse, G. & Joubert, D. From ultrasoft pseudopotentials to the projector augmented-wave method. *Phys. Rev. B* **59**, 1758–1775 (1999).
63. Perdew, J. P., Burke, K. & Ernzerhof, M. Generalized gradient approximation made simple. *Phys. Rev. Lett.* **77**, 3865–3868 (1996).
64. Monkhorst, H. J. & Pack, J. D. Special points for Brillouin-zone integrations. *Phys. Rev. B* **13**, 5188–5192 (1976).
65. Anisimov, V. I., Zaanen, J. & Andersen, O. K. Band theory and Mott insulators: Hubbard *U* instead of Stoner *I*. *Phys. Rev. B* **44**, 943–954 (1991).
66. Mostofi, A. A. et al. wannier90: a tool for obtaining maximally-localised Wannier functions. *Comput. Phys. Commun.* **178**, 685–699 (2008).
67. Marzari, N. et al. Maximally localized Wannier functions: theory and applications. *Rev. Mod. Phys.* **84**, 1419–1475 (2012).
68. He, X., Helbig, N., Verstraete, M. J. & Bousquet, E. TB2J: a Python package for computing magnetic interaction parameters. *Comput. Phys. Commun.* **264**, 107938 (2021).
69. Berry, M. V. Quantal phase factors accompanying adiabatic changes. *Proc. R. Soc. A* **392**, 45–57 (1997).
70. Yu, R. et al. Equivalent expression of Z_2 topological invariant for band insulators using the non-Abelian Berry connection. *Phys. Rev. B* **84**, 075119 (2011).
71. Altland, A. & Zirnbauer, M. R. Nonstandard symmetry classes in mesoscopic normal-superconducting hybrid structures. *Phys. Rev. B* **55**, 1142–1161 (1997).
72. Xu, Q.-R. et al. Squaring the fermion: the threefold way and the fate of zero modes. *Phys. Rev. B* **102**, 125127 (2020).
73. Zhang, M.-H., Xiao, L. & Yao, D.-X. Topological magnons in a collinear altermagnet. Preprint at https://arxiv.org/abs/2407.18379 (2024).
74. Pershoguba, S. S. et al. Dirac magnons in honeycomb ferromagnets. *Phys. Rev. X* **8**, 011010 (2018).
75. Zhang, L., Ren, J., Wang, J.-S. & Li, B. Topological magnon insulator in insulating ferromagnet. *Phys. Rev. B* **87**, 144101 (2013).
76. Mook, A., Henk, J. & Mertig, I. Edge states in topological magnon insulators. *Phys. Rev. B* **90**, 024412 (2014).
77. Owerre, S. A first theoretical realization of honeycomb topological magnon insulator. *J. Phys. Condens. Matter* **28**, 386001 (2016).
78. Mook, A., Plekhanov, K., Klinovaja, J. & Loss, D. Interaction-stabilized topological magnon insulator in ferromagnets. *Phys. Rev. X* **11**, 021061 (2021).
79. Lu, Y.-S., Li, J.-L. & Wu, C.-T. Topological phase transitions of Dirac magnons in honeycomb ferromagnets. *Phys. Rev. Lett.* **127**, 217202 (2021).

Acknowledgements This work was supported by the National Key R&D Program of China under grant number 2020YFA0308900, the National Natural Science Foundation of China under grant number 12274194, Guangdong Provincial Key Laboratory for Computational Science and Material Design under grant number 2019B030301001, Guangdong Provincial Quantum Science Strategic Initiative (grant numbers GDZX2401002 and GDZX2201001), Shenzhen Science and Technology Program (grant numbers RCJC20221008092722009 and 20231117091158001), Innovative Team of General Higher Educational Institutes in Guangdong Province (number 2020KCXTD001), the Science, Technology and Innovation Commission of Shenzhen Municipality (number ZDSYS20190902092905285), the Open Fund of the State Key Laboratory of Spintronics Devices and Technologies (grant number SPL–2407) and Center for Computational Science and Engineering of Southern University of Science and Technology.

Author contributions Q.L. conceived the work. X.C., J.R. and J.L. constructed the group structures and the band representation theory. X.C. and Y.Y. established the database. Y.Y. built the website. X.C., Y.L., P.L. and A.Z. performed the high-throughput DFT and Wannier calculations. X.C. performed the magnon band calculations. X.C. and Q.L. analysed the results and wrote the paper.

Competing interests The authors declare no competing interests.

Additional information

Supplementary information The online version contains supplementary material available at https://doi.org/10.1038/s41586-025-08715-7.

Correspondence and requests for materials should be addressed to Qihang Liu.

Peer review information *Nature* thanks the anonymous reviewers for their contribution to the peer review of this work. Peer reviewer reports are available.